Review

International Journal of Modern Physics B
Vol. 24, No. 31 (2010) 6013–6042

DOI: 10.1142/S0217979210057456

World Scientific
www.worldscientific.com

OPTICAL PROPERTIES AND KINETIC ROUGHENING INFLUENCE ON DISPERSIVE CASIMIR AND VAN DER WAALS FORCES

G. PALASANTZAS*,†, V. B. SVETOVOY‡ and P. J. VAN ZWOL*,§

*Materials Innovation Institute and Zernike Institute for Advanced Materials, University of Groningen, 9747 AG Groningen, The Netherlands
‡MESA and Institute for Nanotechnology, University of Twente, PO 217, 7500 AE Enschede, The Netherlands
†g.palasantzas@rug.nl
‡V.Svetovoy@ewi.utwente.nl
§petervanzwol@gmail.com

Received 7 December 2010

Casimir and van der Waals dispersive forces between real material surfaces can be strongly influenced by surface roughness and the frequency dependent dielectric functions of the interacting materials. The Lifshitz theory allows calculations of these forces between two flat plates if the frequency dependent dielectric function is known. Even in this case in order to compare different measurements of the Casimir force the accuracy must be higher than the force uncertainty arising as a result of the variation in the measured dielectric functions for a given material. Therefore, when we are dealing with dispersive forces between real materials, precise characterization of the particular interacting samples is critical. For this reason the effects of optical properties and surface roughness on dispersive forces will be first discussed in this review paper. Finally, we will compare research results among various research groups, at relatively large surface separations where roughness plays insignificant role, in order to show the level of consensus that has developed in this field in the recent years.

Keywords: Casimir force; van der Waals force; surface roughness; optical properties.

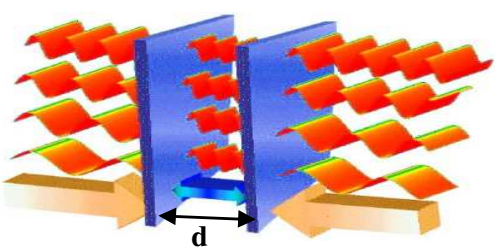

1. Introduction

In the 1940s, Overbeek and Verwey at Philips Research Laboratories in Eindhoven, The Netherlands, accurately measured the attractive van der Waals (vdW) force which acts between all atoms, molecules and small particles due to fluctuations in their electron clouds. Although this force was thought to be explained by the quantum-mechanical theory of Fritz London, Overbeek and Verwey found that at separations beyond a few nanometers the attractive force decreases faster than the theory of London predicted. Overbeek suspected that the difference was caused by the finite speed of light; a fluctuation in the electromagnetic (EM) field from one of the bodies cannot be felt by the other before the time it takes an EM wave to propagate between them. This phenomenon is called retardation. In 1948, Casimir and Polder calculated how retardation alters the force.[1] Later that year, Casimir also derived an equivalent expression for the attractive force between two *perfect* mirrors due to perturbation of the vacuum fluctuations of the EM field (Fig. 1).[2]

Later on, in the 1950s, Lifshitz and his co-workers, Dzyaloshinskii and Pitaevskii,[3] generalized the work of Casimir, accounting for absorption of the EM radiation by real materials, and extending the new theory to materials with arbitrary dielectric functions at arbitrary separations and temperature. Since this contribution, known as the Lifshitz theory, it has been established that the frequency dependent dielectric functions of the materials can significantly affect the Casimir force. The theory correctly describes the attractive interaction due to quantum fluctuations, covering both the Casimir (long-range; separations larger than 20 nm) and van der Waals (short-range; separations shorter than 10 nm) regimes.

Interest in the Casimir force was intensified shortly after Lamoreaux's landmark experiment in 1997, where a torsional pendulum was used for high accuracy force

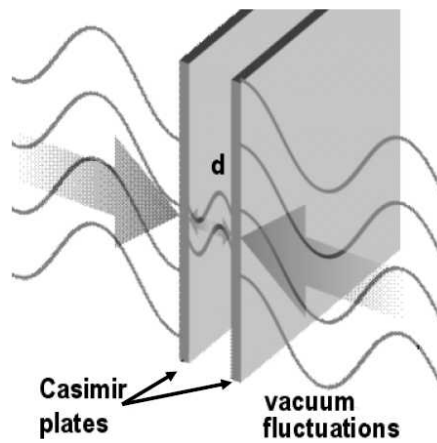

Fig. 1. Casimir force seen as a result of quantum vacuum fluctuations. The narrow space d between plates excludes fluctuations of wavelength $> 2d$, thereby inducing a pressure difference between the internal and external space resulting in an attractive force pushing the plates together.

measurements.[4] Later on atomic force microscopy (AFM) was also used in experiments.[5] Independent of the measuring technique, two obstacles hinder comparison between the measured and calculated Casimir force at short separations (< 200 nm) where the force is relatively strong:

(1) *Surface roughness*:[6] The Casimir force can strongly depend on surface roughness depending on the separation distance over which the force is calculated or measured. In reality nanoscale surface roughness can have a significant effect at separations below the plasma wavelength (e.g., for Au this is ~ 137 nm). An important parameter influencing the Casimir force is the surface roughness amplitude, which for deposited thin film surfaces, used in both force measurements and applications, can vary typically from 0.5–10 nm (or even more). Figure 2 shows AFM topography scans of deposited metal films used for optical characterization, roughness studies and force measurements.

(2) *Optical properties*: Real materials are imperfect conductors (dielectrics).[7] The dielectric properties strongly influence the Casimir force especially at separations below the plasma wavelength. For an accurate calculation of the Casimir/vdW force between real materials, the frequency dependent dielectric

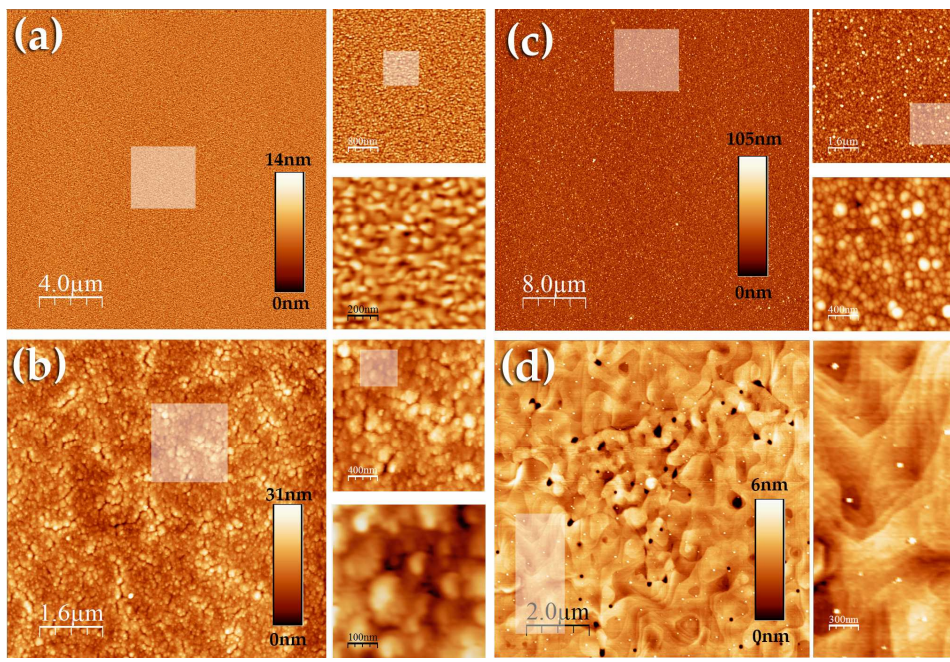

Fig. 2. AFM topography scans (with up to 4000×4000 pixels for the largest scan size) of gold surfaces where the highlighted areas are magnified. The color scale bars apply only to the large images. (a) 100 nm Au on Si, (b) Au coated polysterene sphere (first plasma sputtered then 100 nm Au evaporated, (c) 1600 nm Au on Si, (d) very high quality 120 nm Au on mica, annealed for a few hours and slowly cooled down.

function *must* be obtained experimentally and used as input, as for example the Lifshitz theory dictates.[8]

In the following we will analyse in more detail the optical properties and surface roughness in order to attain a clear understanding on the limitations and advantages that bring into the knowledge of Casimir/vdW forces between real materials.

2. Optical Properties and Lifshitz Theory

2.1. *Analysis of optical properties*

Although it is preferable to use in force measurements macroscopic perfect single crystals,[9] whose optical properties could be calculated using quantum physics,[10] in reality perfect single crystals do not exist on macroscopic length scales. Nonetheless, the semiconductor industry is capable of producing single crystal silicon or germanium samples with very low defect and/or impurity densities.[11] However, most Casimir force measurements and of course the corresponding optical characterization (measurement of the frequency dependent dielectric function) are performed between metal surfaces of vacuum deposited (e.g., electron-beam evaporated, plasma sputtered, etc.) films.[7,8,12–15] Although the surface morphology of the smoothest film is atomically smooth over various length scales [with atomic steps and terraces visible, Fig. 2(d)], local trenches of 5 nm deep are still present. These films are granular, where the grains are rather small of the order of tens of nanometers, and the amount of defects (voids, grain boundaries, impurities) can be very large.[8]

The presence of defects in deposited thin films has influence on the Casimir/vdW force. A detailed study[7] revealed that scatter in the dielectric data can lead up to 8% uncertainty in theory calculations using the Lifshitz theory.[3] Most of the optical data available for metals do not extend beyond the wavelength of 14 μm in the infrared (IR) range.[13,14] It was only recently[8] where ellipsometry from the far infrared (IR) to near ultra violet (UV) was used over the frequency range 140 nm–33 μm to obtain the frequency dependent dielectric function for gold films. The dielectric response of a material for the UV (> 5 eV), IR (0.01–1 eV) and microwave (MW) (0.0001–0.01 eV) is related to electronic (band) resonance, atomic resonance (for metals this is the electron cloud) and dipole relaxation respectively.

The optical properties of materials[13] are described by two measurable quantities: the index of refraction $n(\lambda)$ and the extinction coefficient $k(\lambda)$, which both depend on the wavelength λ of the electromagnetic radiation. They define the complex index of refraction $\tilde{n} = n + ik$. The real part defines the phase velocity in a medium $\nu = c/n$ where c is the velocity of light, while the imaginary part is related to light that is adsorbed when it travels through the medium. The real and imaginary parts of the frequency dependent dielectric functions are determined from n and k via the relations $\varepsilon' = n^2 - k^2$ and $\varepsilon'' = 2nk$ (see Fig. 3). Both pairs (n, k) and $(\varepsilon', \varepsilon'')$ must obey causality and as a result must satisfy the Kramers–Kronigs (KK)

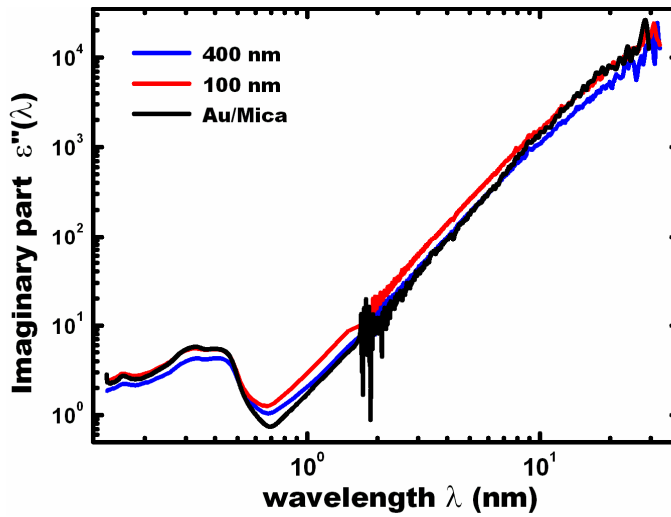

Fig. 3. Ellipsometry data of the dielectric function as a function of frequency of three gold films on Si and mica. The annealed film on mica has the highest reflection (in the infrared), and the 400 nm thick film on Si (not annealed) the lowest. The differences are not that visible here, but the deviations from sample to sample can be as large as 40%.

relations.[7,8,13] In many cases, only the absorption ε'' is measured. This appears to be sufficient because in the Lifshitz theory one has to know the dielectric function at imaginary frequencies $\varepsilon(i\zeta)$ which is defined as

$$\varepsilon(i\zeta) = 1 + \frac{2}{\pi}\int_0^{+\infty} \frac{\omega\varepsilon''(\omega)}{\omega^2+\zeta^2} d\omega\,. \tag{2.1}$$

It is also possible to obtain the dielectric function at imaginary frequencies directly from the frequency dependent extinction coefficient k since $\varepsilon(i\zeta) = n(i\zeta)^2$ with

$$n(i\zeta) = 1 + \frac{2}{\pi}\int_0^{+\infty} \frac{\omega k(\omega)}{\omega^2+\zeta^2} d\omega\,. \tag{2.2}$$

Although the latter is very useful in dealing with experimental dielectric data, one should be careful when using the KK relations since in most cases dielectric data is available over a limited frequency interval and not in the full range $[0, +\infty]$ as required by Eqs. (2.1) and (2.2). As a result specific assumptions must be made about the form of the dielectric data outside of measurement intervals, or the data should be combined with other (tabulated) experimental data. For example, in the case of gold films one needs to fit a Drude model in the far IR regime. For gold the IR absorption ε'' is strong and dominates the dielectric function at imaginary frequencies $\varepsilon(i\zeta)$ even in the UV regime (Figs. 3 and 4). On the other hand, for silica and liquids the dielectric function in the far IR and MW regimes is up to 10^8 times smaller than that of Au (Fig. 4).[16] In this case, the IR and MW parts of the dielectric data give an almost negligible contribution to the integrals in the KK relation for $\varepsilon(i\zeta)$ in the UV regime. Instead, the UV dielectric data for ε'' is

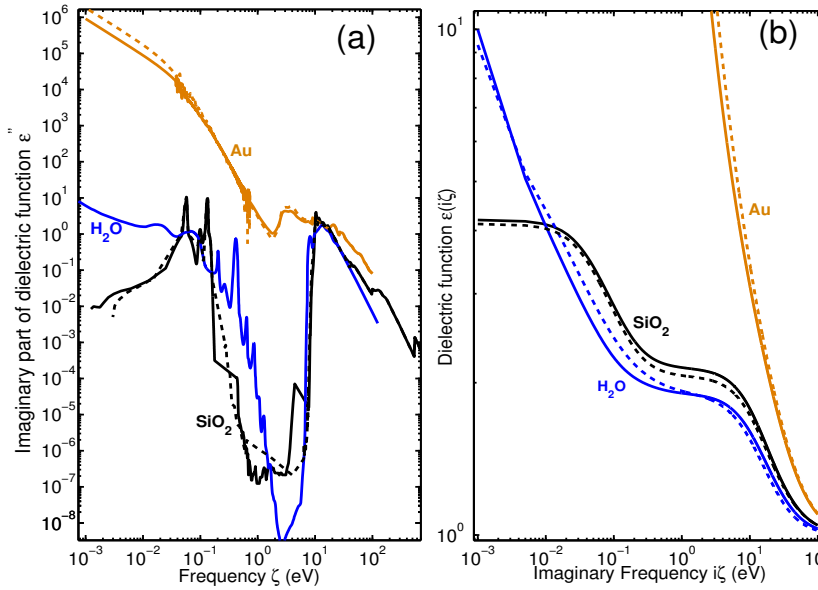

Fig. 4. (a) Dielectric data of the materials obtained from references in text. (b) Dielectric functions at imaginary frequencies. The solid and dashed lines for silica and gold are two different sets of optical data. For water the solid line is from the data in Ref. 22, and the dashed line is an 11-order oscillator model which has been fitted to a different set of optical data.

very important as illustrated in Fig. 4, the absorptive part of ε'' in the UV regime is not very different for gold and silica, while $\varepsilon(i\zeta)$ shows significant difference.

Ellipsometry is a non-destructive technique to measure the dielectric function. In this case one measures an intensity ratio between incoming and reflected light. Therefore, it is less affected by intensity instabilities of the light source or atmospheric absorption, and no reference measurement is necessary. Moreover, both the real and imaginary parts of the complex refractive index can be extracted. Indeed, from ellipsometry we obtain the ratio of the p-polarized and s-polarized complex Fresnel reflection coefficients $r_{p,s}$.[17,18] This is given by $\rho = r_p/r_s = \tan\psi e^{i\Delta}$ with the angles ψ and Δ being the raw data as a function of the wavelength λ. When the films are completely opaque, $r_{p,s}$ are given by

$$r_p = \frac{\varepsilon\cos\varphi - \sqrt{\varepsilon - \sin^2\varphi}}{\varepsilon\cos\upsilon - \sqrt{\varepsilon - \sin^2\varphi}}, \quad r_s = \frac{\cos\varphi - \sqrt{\varepsilon - \sin^2\varphi}}{\cos\varphi - \sqrt{\varepsilon - \sin^2\varphi}} \tag{2.3}$$

where φ is the angle of incidence, and $\varepsilon = \langle\varepsilon(\lambda)\rangle$ is the film "pseudodielectric" function. The term "pseudo" indicates that the films can be anisotropic and nonuniform, have surface roughness (Fig. 2), and also contain absorbed layers (water, hydrocarbons, etc.) if they are exposed to ambient conditions. The dielectric function extracted from the raw data can be influenced by these factors.

For gold films typically used in force measurements, we do not expect that these factors will have large effect because gold absorbs strongly in the IR, and surface

roughness (< 10 nm rms) is significantly smaller than the smallest wavelength of 137 nm of the ellipsometry measurements.[8] For an isotropic and uniform solid, the dielectric function is connected with the parameter ρ via the relation

$$\varepsilon = \varepsilon' + i\varepsilon'' = (n + ik)^2 = \sin^2\varphi \left[1 + \tan^2\varphi \left(\frac{1-\rho}{1+\rho}\right)^2\right]. \tag{2.4}$$

As it was stated before, the largest spectral range of measured data is 137 nm to 33 μm.[8] In order to obtain $\varepsilon(\omega)$ for wavelengths $\lambda > 33$ μm where data is not available, we fit a model to the IR part[8] and extrapolate (for the far UV regime $\lambda < 137$ nm we use handbook data[7] though the latter gives only a minor contribution to the Casimir force in case for example of gold).[8]

Ellipsometry in the range of wavelengths $\lambda > 33$ μm is difficult due to lack of intense sources, but these systems are still in development.[19] For gold films it would be extremely interesting to have dielectric data in this regime because fitting and extrapolating will then be almost unnecessary.[8] On the other hand, dielectric data obtained by ellipsometry or absorption measurements[20] in the far UV regime is also rare. These measurements are expensive because high energy photons must be produced at synchrotrons,[21] and ellipsometry in this range is complicated as polarizing materials become non-transparent. For this range, a few ellipsometry setups exist around the world covering the range 5–90 eV (wavelength $\sim$200–12 nm).[21] For low dielectrics such as all liquids, and for example silica or teflon, there is a major absorption band in the range 5–100 eV (Fig. 4), which dominates the calculations of the Casimir force for these materials.

2.2. *Analysis of optical properties for gold*

At this point, we will take a closer look at the dielectric functions of gold films which are the most commonly used for Casimir force measurements (Fig. 3). In this case, we fitted a Drude model to this data to obtain data for the wavelength range $\lambda > 33$ μm where measured dielectric data is not available. The Drude model for metals is described by two parameters: the plasma frequency ω_p of the free electron cloud, and the electron-lattice scattering via a relaxation parameter γ. In general, the model fitted to the data reads of the form

$$\varepsilon(\omega) = E - \frac{\omega_p^2}{\omega(\omega + i\gamma)}. \tag{2.5}$$

For metals, e.g., Au, we have $E = 1$ but for systems in between metal-semiconductors, E can be treated as a fitting parameter representing contributions other than free electrons. In any case, it is obvious that there is a large variation in dielectric data for all gold films studied up to 40%.[8] Furthermore, we find the highest optical response for the annealed films on mica for which we have found the highest plasma frequency of 8.4 eV. This is close to but smaller than the theoretical limit $\omega_p = 9$ eV for a perfect single crystal gold sample.[22]

Note that all metals have finite conductivity. It means that at low frequencies $\omega \to 0$ the dielectric function behaves as $\varepsilon(\omega) \to 4\pi\sigma/\omega$, where σ is the material conductivity. This behaviour is a direct consequence of Ohm's law and therefore has fundamental character. Indeed, because the dielectric function has a pole at $\omega \to 0$, the low frequencies will give a considerable contribution to $\varepsilon(i\zeta)$ even if ζ is high (for example, in the visible part of the spectrum) as one can see from Eq. (2.1).

2.3. *Lifshitz theory for flat surfaces: Influence of optical properties*

The Casimir force is calculated using the dielectric function at imaginary frequencies (Fig. 5). For the sphere-plate geometry, which is typically used for force measurements, the Casimir force is given by $F = 2\pi R E_{p-p,f}$ assuming that the sphere radius R is much larger than the sphere-plate separation d ($R \gg d$), with $E_{p-p,f}$ the Casimir energy for the plate-plate geometry. The Lifshitz theory yields for the Casimir energy $E_{p-p,f}$ between flat surfaces of area A (in the limit of $T = 0$ K; which is a good approximation for $d < 200$ nm)

$$E_{p-p,f} = \frac{\mathbf{h}}{2\pi} A \sum_p \int \frac{d^2q}{(2\pi)^2} \int_0^\infty \ln[1 - r_{31}^p r_{32}^p e^{-2\kappa_3 L}] d\zeta \,. \tag{2.6}$$

$\mathbf{q}$ is the transverse wave vector ($q = |\mathbf{q}|$). The summation p here is defined for the polarization of the field, i.e., transverse magnetic and electric field modes ($p = TM$ and $p = TE$). The reflection amplitudes r_{3i}^p are given by the Fresnel reflection

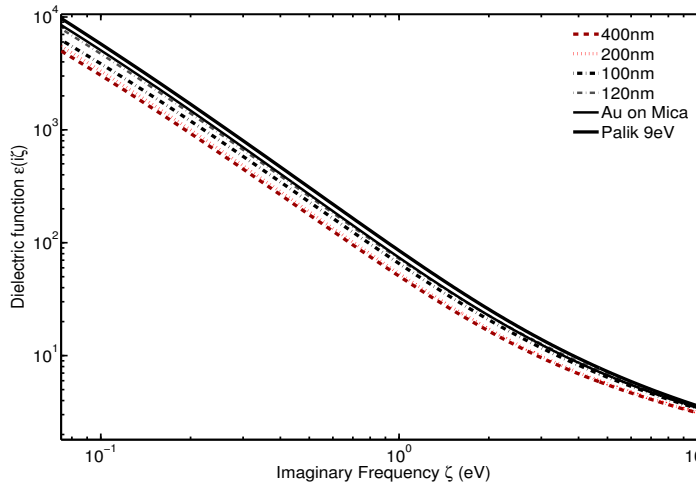

Fig. 5. The dielectric function for various films at imaginary frequency which can be substituted into the Lifshitz theory. This non-observable function can be obtained by Kramers–Kronig analysis of ε'' of which the infrared part has the most influence on $\varepsilon(i\zeta)$. The films are the same as in Fig. 3. The function marked as Palik 9 eV correspond to an imaginary film with Palik optical data and the maximal plasma frequency 9 eV.

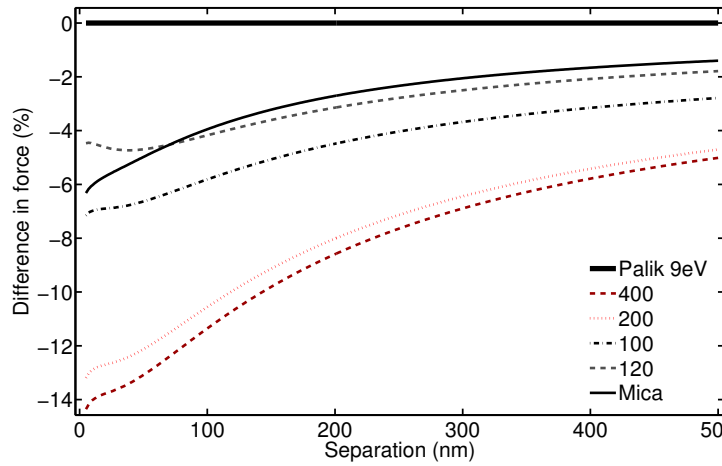

Fig. 6. The Casimir force differences between our films and an imaginary film with Palik handbook data fitted with a plasma frequency of 9 eV. Sample dependence of the force is visible, with the highest force for the Au on annealed mica sample. At a separation of a micron the difference is still a few percent.

coefficients

$$r_{3,i}^{\mathrm{TE}} = \frac{\kappa_i - \kappa_3}{\kappa_i + \kappa_3} \quad r_{3,i}^{\mathrm{TM}} = \frac{\kappa_i \varepsilon_3 - \kappa_3 \varepsilon_i}{\kappa_i \varepsilon_3 + \kappa_3 \varepsilon_i} \text{ and } \kappa_i = \sqrt{q^2 + \frac{\varepsilon_i(i\zeta)\zeta^2}{c^2}} \tag{2.7}$$

where $\varepsilon_{1,2}$ are the dielectric functions for the interacting solid surfaces, and ε_3 is the dielectric function for the intervening medium between the sphere and plate.

The Casimir force for the Au films interacting in air, and normalized with respect to that calculated from the handbook data fitted with a Drude function for perfect gold ($\omega_p = 9$ eV, $\gamma = 0.034$ eV),[8,13] is shown in Fig. 6 for all films with measured optical properties.[8] The difference in force is obvious. The annealed gold film on mica shows the largest Casimir force, and approaches that of perfect gold films with only 5% difference. The 400 nm thick film on Si has the lowest Casimir force with up to 14% difference from the perfect gold film. At last we note that due to the error indefiniteness in the Drude parameters, we obtain an error of $\sim 1\%$ in the calculated Casimir force.

Furthermore, an important question is whether the investigated films follow the Drude behavior in the IR regime as can be seen from Fig. 7. Indeed, the Drude model must obeys a linear behavior in $1/\varepsilon'$ versus $\omega^2+\gamma^2$ plot. This becomes evident if one considers the real and imaginary parts of Eq. (2.5). The Drude model fits almost perfectly the gold film/mica data, but for the 200 nm unannealed Au film there is a significant deviation for the wavelength range above 15 μm. This deviation was visible for all the non-annealed films, and it was smaller for the film with higher optical quality (plasma frequency). From this it is concluded that there is additional absorption due to defects (grain boundaries, voids, dislocations, etc) as discussed in Ref. 8. Moreover, at large wavelengths the experimental data also becomes noisier

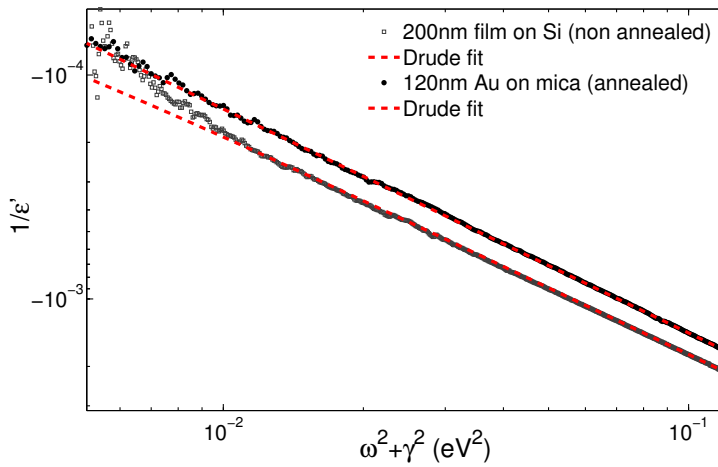

Fig. 7. The Drude model must show a linear behavior in a $1/\varepsilon'$ versus $\omega^2 + \gamma^2$ plot. In the low frequency range ($\lambda > 15$ μm), a clear deviation is visible for the non-annealed film. This effect was not taken into account in the Casimir force calculations. The non-Drude behavior becomes weaker for the films with better quality, and is the smallest for the gold film on mica. This leads to the conclusion that the non-Drude behavior can be attributed to the number of defects in the films (grain boundaries, dislocations, etc).

leading to an error of 1% in the calculated forces.[8] The non-Drude behavior for the force calculations could be fitted with an additional oscillator model, but it gives a contribution in the order of 1% in the calculated forces, which is similar to the noise level.[8]

3. Roughness of Real Materials and the Casimir/vdW Force

In order to account for roughness corrections on the Casimir force, a scattering formalism was presented[23] in the limit of weak roughness (local surface slope $|\nabla h| \ll 1$ and surface separations $d \gg w$). Here we will discuss this theory using measured Casimir forces and topography roughness scans.[24] Note that the Proximity Force Approximation (PFA) method uses only the rms roughness "w" (out-off plane roughness) to predict the roughness effect.[25] While this is the most important factor, any lateral information of the rough films is ignored.[23]

3.1. *Roughness influence on the Casimir/vdW force*

The force between rough surfaces in the sphere-plate geometry is given again by the PFA expression $F = 2\pi R E_{p-p,r}$ with $E_{p-p,f} + \delta E$ the Casimir energy for parallel plates. The Lifshitz theory, Eq. (2.6), yields the energy $E_{p-p,f}$ between flat surfaces, while the roughness contribution up to the second order in perturbation theory reads of the form[23]

$$\delta E = \int G(k)\sigma(k)\frac{d^2k}{4\pi^2}\,. \tag{3.1}$$

$G(k)$ is a roughness response function derived in Ref. 23. The roughness power spectrum $\sigma(k)$ can be obtained from AFM topography scans. We should also recall that for these calculations to be valid a few assumptions were made: (i) The lateral dimensions of the roughness must be much smaller than the system size (i.e., plate or sphere). This is usually the case in the experiment. (ii) Second, the RMS roughness must be small compared to the separation distance ($w \ll d$). (iii) Third, lateral roughness dimensions must be much larger than the vertical dimensions, or conversely the local surface slope of a film must be small ($\rho_{\mathrm{RMS}} = (\langle|\nabla h|2\rangle)^{1/2} \ll 1$).[26,27] The last two assumptions are not always satisfied in the experiment.[24]

Evaporated thin films can be described in many cases by the self affine or power law roughness.[28] The importance of self affine scaling and the relation to the Casimir force was first stressed in Ref. 26, but finite conductivity corrections were ignored. Here finite conductivity corrections are taken into account since we used measured optical data for the gold films. Roughness data is taken from gold films evaporated on Si and the spheres. A self affine rough surface is fully characterized by three parameters, the rms roughness w, the correlation length ξ, which is a factor indicating the lateral feature size, and the roughness exponent H which is a factor describing the irregularity of short roughness wavelengths with values between 0 and 1 (Fig. 8).[28–30]

The power spectrum function $\sigma(k)$ can be obtained directly by Fourier transforming the auto covariance function as obtained from AFM topography scans. On the other hand the parameters w, ξ and H are determined by direct measurement of the height-difference correlation function $H(r) = \langle[h(r) - h(0)]^2\rangle$ with $\langle\cdots\rangle$ indicating ensemble average over multiple surface scans. An analytic form of the power spectrum for a self affine surface (suitable for theory calculations) was given in Ref. 29.

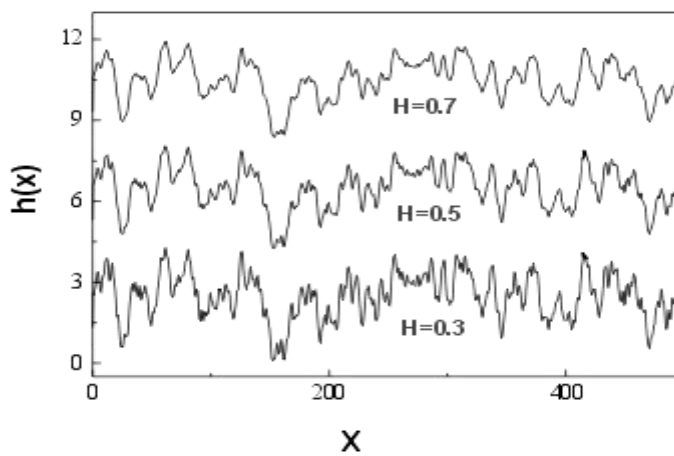

Fig. 8. Roughness profiles with different roughness exponents H but the same w and ξ.

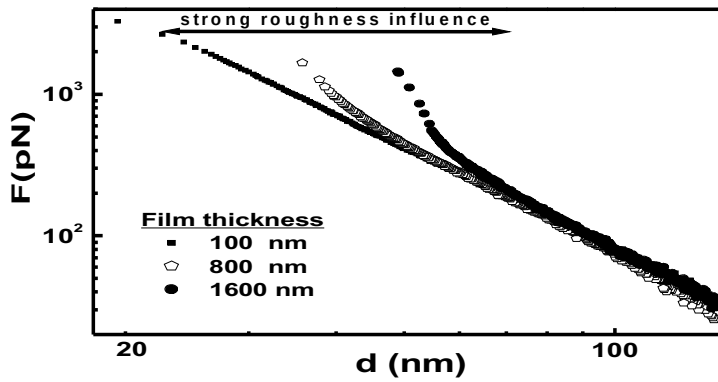

Fig. 9. Casimir force measurements (any curve is an average of 30 curves, immediately taken after calibration) for smoother and rougher films. The jump to contact part of the curves is not shown. The roughness effect manifests itself as a strong change in scaling at smaller separations, where the forces become much stronger. The separation upon contact d_0 in this case was taken from the electrostatic calibration of d_0.[24]

Here we will show force measurements for gold films of different roughness (Fig. 9). These were compared in Ref. 24 to predictions from the perturbative scattering theory, which incorporated measured optical data and roughness corrections in terms of the complete surface roughness spectrum.[29]

For the force measurement the calibration procedure was given in detail elsewhere.[24,32] Table 1 shows some of the roughness data (obtained and averaged from AFM scans on multiple locations) of our films combined with that of the sphere. These data can be used in the scattering theory calculations.[23,24] The roughness exponent was constant $H = 0.9 \pm 0.05$ in agreement with previous growth studies of thin films.[28–30]

The force measurements in Fig. 9 were restricted to separations below 200 nm where the Casimir force is strong enough (as compared to almost linear signal due to laser light backscattered into the AFM photodiode).[5,24,36] The small separation limit is restricted by the distance upon contact d_0 due to surface roughness (substrate and/or sphere roughness),[24] and it is also restricted by the jump to contact instability (which takes place over a separation of ~ 5 nm).[32–34,47,48]

Table 1. The roughness parameters characterizing the sphere-plate film systems (all in nm). The first four rows were determined from combined AFM megascans.[31] $d_0^{\rm el}$ is the value of the distance upon contact due to roughness determined electrostatically, and $d_0^{\rm im}$ is the value determined from AFM topography.[31]

Thickness (nm)	100	200	400	800	1600
w (nm)	3.8	4.2	6.0	7.5	10.1
ξ (nm)	26.1 ± 3.8	28.8 ± 3.7	34.4 ± 4.7	30.6 ± 2.4	42.0 ± 5.5
$d_0^{\rm im}$ (nm)	12.8 ± 2.2	15.9 ± 2.7	24.5 ± 4.8	31.3 ± 5.4	55.7 ± 9.3
$d_0^{\rm el}$ (nm)	17.7 ± 1.1	20.2 ± 1.2	23.0 ± 0.9	34.5 ± 1.7	50.8 ± 1.3

The plane-sphere separation for our contact mode measurement setup is given by $d = d_{\text{piezo}} + d_0 - d_{\text{defl}}$ (measured with respect to the point of contact with the surface), with d_{piezo} the piezo movement, and d_{defl} the cantilever deflection correction.[24] The latter is given by $d_{\text{defl}} = mF_{pd}$ with F_{pd} the photodiode difference signal and m the deflection coefficient (rate of change of the separation per unit photodiode difference signal).[24]

In Fig. 9 we can observe the strong dependence of the Casimir force on surface roughness at separations $d < 70$ nm. For the roughest films, the roughness strongly increases the force. This effect is large, resulting in much stronger forces at the smallest ranges (< 70 nm) while at larger separations the usual $\sim 1/d^{2.5}$ force scaling is recovered (observed for separations above 25 nm for smoother films),[35] and agreement with theory is restored.[24] Deviations from theory at short separations can occur and they can be explained with the error in the separation distance d. Note that an error of 1.0 nm in d leads to significant errors in the forces. This can be seen by the simple formula $\Delta F/F \approx 2.5(\Delta d/d)$ where at the shortest separation distance $d \approx 20$ nm an error of $\Delta d \approx 1 - 1.5$ nm (Table 1) yields a relative error for the force $\Delta F/F \approx 13 - 18\%$,[24] which, however, diminishes with increasing separation.

Qualitatively the roughness effect could be reproduced by performing a direct integration using the Lifshitz formula to compute the force between rough surfaces by point to point (using the AFM topography scans) summation and average over multiple measured roughness scans.[24] Although the non perturbative PFA approach is qualitative, it can be used to obtain an estimate of the force at close proximity (~ 2 nm above the point upon contact d_0), where the roughness has an enormous influence on the Casimir force. This explains the jump to contact only partially, since approximately ~ 5 nm above the point of contact, the capillary force arising from both absorbed water and capillary condensation can play some role.

Here, we can compare the Casimir adhesion between rough films with the capillary adhesion[32–34] (Fig. 10). In the limit of a fully wetted surface the capillary force is given by $F_{\text{cap}} \approx 4\pi\gamma R\cos\theta$ (upper dashed line, Fig. 10), while for single asperity (say of size ξ) wetting, the capillary force is $F_{\text{cap}} \approx 4\pi\gamma\xi\cos\theta$ (lower dashed line, Fig. 10). γ is the liquid surface tension, and θ the contact angle.[33,34] While Casimir forces may lead to stiction between movable parts, once hydrophilic surfaces are in contact in air then capillary forces are much stronger. The roughness effect on the capillary adhesion force (Fig. 10) is also much stronger than that of the Casimir force in Fig. 9. Note that the Casimir force for a $R = 50$ μm sphere is in the order of 10 nN at ~ 10 nm separations, while the capillary forces between a mica substrate (0.5 nm rms roughness) and the same sized sphere (~ 1 nm rms roughness) are as large as 10 μN. The latter makes force measurements (using contact mode) with soft cantilevers (spring constant < 1 N/m) even impossible since the retraction range can be even more than the piezo z-range. Moreover, one can notice in Fig. 10 when increasing the roughness from 2 to 8 nm the force decreases by more than two orders of magnitude. This is due to transition from full sphere wetting to a few

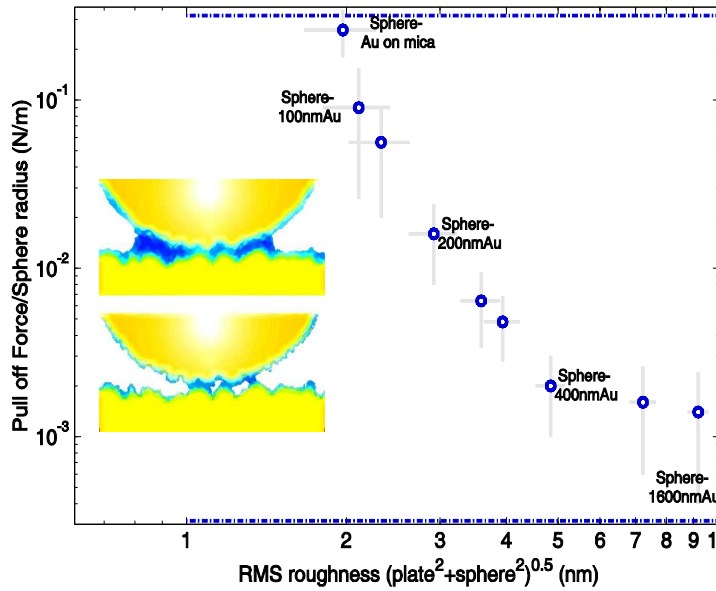

Fig. 10. Capillary, or pull off forces, in air (relative humidity 2–60%, no significant variation beyond the standard deviations was found in this range) for a smooth gold coated 100 μm sphere ($\sim$1 nm rms roughness) measured with a stiff cantilever ($k = 8$ N/m) and different rough films. The inset shows a fully wetted sphere, and a roughness asperity wetted sphere. The fully wetted corresponds to the theoretical strong pull off force (upper dashed line), and the single asperity wetted to the weak pull off forces (lower dashed line).

asperity wetting. The size of the sphere $R = 50$ μm is 10^3 times larger than that of an asperity ($\sim$50 nm in size and comparable to the lateral correlation length ξ, see Table 1). Multiple asperity capillary bridge forming is likely to take place in the rough regime giving rise to forces larger than that of a single asperity.

Furthermore, formation of capillary bridges means that under ambient conditions, a metal surface such as gold absorbs water, and as a result is covered with an ultra thin water layer (which is present on almost all surfaces exposed to air). The experiment[33,34] suggests that the thickness of this layer is in the nanometer range $\sim 1-2$ nm. At short separations, $d < 20$ nm, this layer becomes of crucial importance because it place doubts in our understanding of Casimir/vdW forces when experiments under ambient conditions are compared with predictions of the Lifshitz theory. Figure 11 shows the Casimir force measurements together with theory calculations for various water layers of thickness $h = 0$; and 1.5 nm.[36] The effect of water becomes very significant at separations below 10 nm, which unfortunately were not accessible due to jump-to-contact at approximately 12 nm separations. We presented in Fig. 11 only the forces between flat surfaces because at these small separations, there is not yet a reliable way to estimate the roughness correction. Furthermore, the theoretical predictions are comparable to the experimental measurements for distances $d \geq 13$ nm (limited only due to strong jump-to contact by

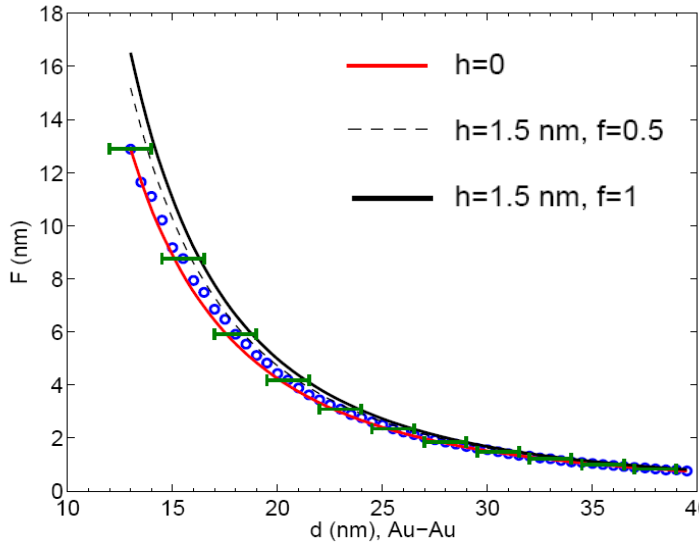

Fig. 11. Experimental data for the force versus distance (circles) down to 13 nm separations, and the theoretical prediction without water layer (lower solid curve). Errors in the absolute separation (due to errors in d_0) are shown for some points by the bars. The upper solid curve is the prediction for continuous water layer of thickness $h = 1.5$ nm. The dashed black curve corresponds to the same water layer with ($f =$) 50% of voids.

formation of capillary bridges). It is shown that although the water layer increases the force, it falls still within the error margins of the measured force. The errors are shown to arise mainly from the experimental uncertainty in determining the separation upon contact d_0 due to nanoscale surface roughness,[36] which we will analyze in the following paragraph.

3.2. *Roughness influence on surface separation between interacting bodies*

The distance between two rough surfaces is defined as the distance between their mean heights. One would expect that the mean height is a constant when the size L of the sample area of a rough surface is $L \gg \xi$. In the case of a sphere above a plate there is the scale L that is defined by the effective interaction area $L^2 = \alpha\pi Rd$ ($\alpha = 2$ for the electrostatic force and $\alpha = 2/3$ for the ideal Casimir force) where R is the sphere radius, and $d = d_0$ the closest separation distance between sphere and plate. For a sphere of $R = 50$ μm located above a plate this effective interaction area is ≥ 1 μm for $d \geq 10$ nm. Notably, the effective interaction area, and thus the involved mean height on the surface for the electrostatic force, which is used for electrostatic calibration in Casimir force measurement setups, is different from that of the Casimir force.[31] Moreover, it is important to realize that the effective interaction area changes with distance thus introducing an error. This effective error in separation d can be ~ 1 nm as can be seen from Fig. 12.

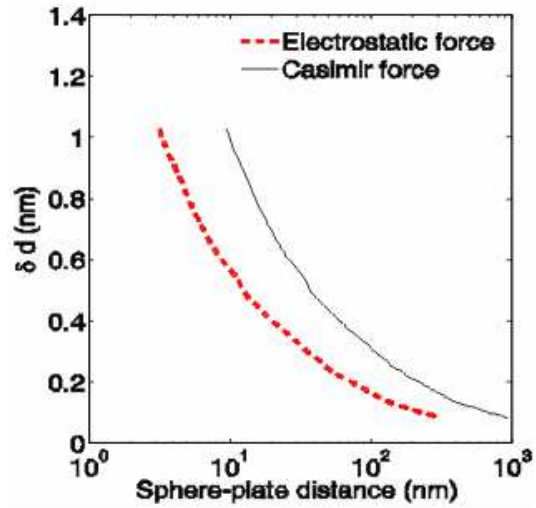

Fig. 12. For the electrostatic force and Casimir force there is an additional error in the distance due to change of the effective interaction area with distance. Since both forces scale differently (electrostatic $\sim 1/d$ and ideal Casimir $\sim 1/d^3$) the effective interaction area, and therefore the involved mean height can be different for these two forces.

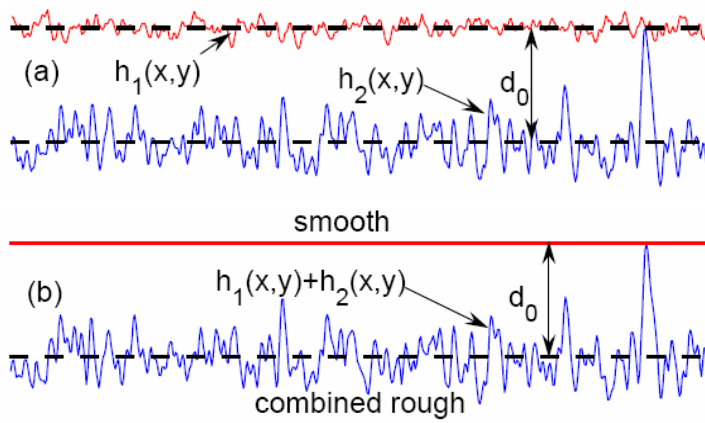

Fig. 13. Contact of two rough surfaces. (a) Two rough plates in contact. (b) The interaction between two rough plates is equivalent to the interaction between a smooth plate and a rough plate with the roughness given by the combined profile $h(x; y)$.[36]

A variation in the mean height of a surface influences both non-contact[37] and contact[24] type Casimir force measurement setups. As stated earlier, the surface roughness leads to a minimum distance upon contact between the mean heights of two rough profiles termed as d_0 (Fig. 13).[24,36]

The contact distance d_0 is not directly measured in non-contact force measurements (the distance between two mean heights is calibrated), while for contact force

measurements, it can also be obtained from electrostatic force measurements.[24] We can compare these values (Table 1)[36] obtained from electrostatic with the values obtained from the measured roughness scans shown in Fig. 2 by performing simulations.[36]

Indeed, the local distance $d(x, y)$ between two rough bodies with height profiles $h_{1,2}(x, y)$ is given by $d(x, y) = d - h(y, y)$ (Fig. 13) where $h(y, y) = h_1(y.y) + h_2(y, y)$ is the combined height profile, and d is the average distance between the mean planes. For a sphere and a plate we have, assuming $R \gg d$, the local distance in the limit of zero load is given by $d(x, y) = d + (x^2 + y^2)/2R - h(y, y)$.[36] The separation upon contact d_0 is the maximum separation d, for which the local distance is $d(x, y) = 0$. This definition gives

$$d_0 = \max_{x,v}[h(y, y) - (x^2 + y^2)/2R] \,. \tag{3.2}$$

As input data we used the combined AFM images, of which a few are shown in Fig. 2, and then d_0 was calculated (Fig. 14). We averaged d_0 over different locations to obtain the values of d_0^{im} (Table 1).[36]

Figure 14 depicts simulation (d_0^{im}) and theory for the sphere-plate system with $R = 50$ μm. d_0 depends on the scan size and increases with that. This is shown for the 100 nm Au film. From this graph one can see that the interaction area upon contact must be approximately 1 μm^2. For the latter we have found d_0 to be about 13 nm from the simulations. For bigger spheres with the same roughness (Fig. 15), d_0 will further increase. The reason for this is that for a rough film, the larger interaction area means an increased possibility to find a higher surface feature.[36]

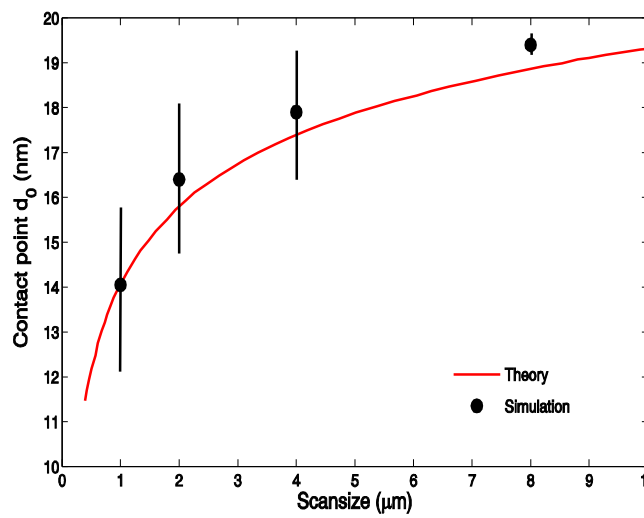

Fig. 14. The contact point as a function of the scan size, for the 100 nm film and the flattened scan of the sphere (see Fig. 2). The separation upon contact increases with scan size. The continuous red line depicts the theory as described in detail in Ref. 36.

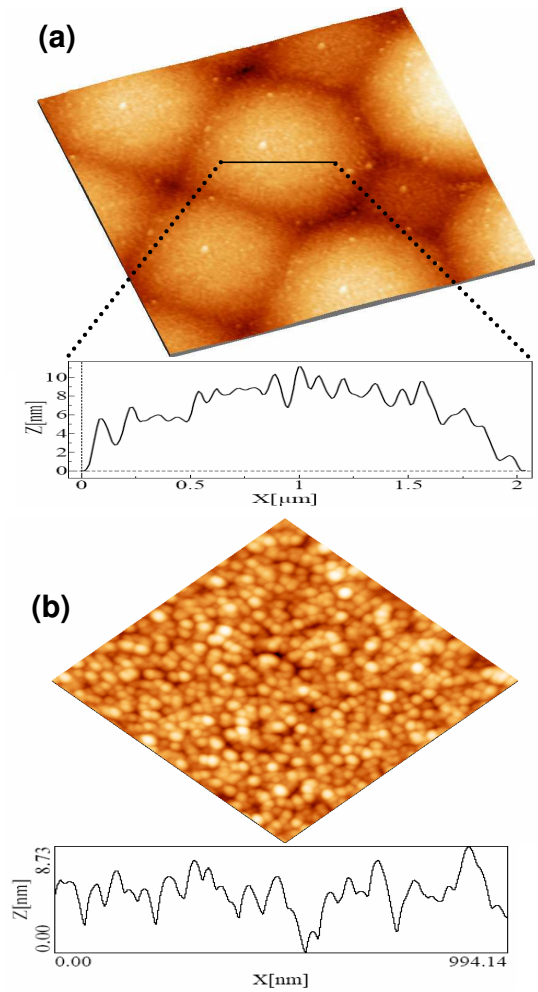

Fig. 15. (a) Inverse imaging of the sphere area (after Au deposition) around which contact with the surface occurs during force measurement. (b) AFM topography with a scan size of 1 μm, and an associated height profile indicative of the roughness variations for the smoothest deposited Au films for short range force measurements.[35]

As can be seen from Table 1, the values of $d_0^{\rm im}$ from the simulations agree well with those from the electrostatic calibration ($d_0^{\rm el}$) except for the smoothest surfaces. This is most likely to be attributed to the roughness on the sphere (Fig. 15) which varies locally significantly. This is illustrated by the fact that when the roughness of the plate dominates, the discrepancy between the simulation ($d_0^{\rm im}$) and electrostatic determination ($d_0^{\rm el}$) disappears. Note that the standard deviations from the simulations using AFM scans are larger than that of the electrostatic determination. This is because for the simulation there is a variation from place to place. For the electrostatic determination this was not performed (since also the rough area for

sphere always remains the same). The error shown for d_0^{el} originates only from a variation obtained from 60 electrostatic curves.[36,37]

4. Beyond the Roughness Influence: Qualitative Comparison of Force Measurements

Beyond the regime of short separations where roughness no longer has influence on the Casimir force, but only on optical properties, we can gain a clear understanding of the extent where Casimir force measurements from various groups agree. For this purpose, we will present force data versus separation where the corresponding average power law exponent of the Casimir force will be stated. Indeed, in this case the Casimir force appears to behave as an apparent power law of the form

$$F \propto d^{-m} \tag{4.1}$$

with $m < 3$ for the sphere-plate geometry due to the influence of the optical properties of the interacting real materials, and the finite system temperature. In the ideal case ($T = 0$ K and perfectly reflecting surfaces) the exponent m has the limiting value $m = 3$.[1–6] If the derivative of the force is measured (e.g., in dynamic mode force measurements), then we obtain the power law form $\partial F/\partial d \propto d^{-(1+m)}$. It should be pointed out that, in a strict sense, the Casimir force shows a more complex behavior than that described by Eq. (4.1), where the local value of the exponent m varies with separation distance from $m = 2$ for very small distance $d \sim 1$ nm to the asymptotic values $m = 3$[1–6] for separations $d > 1$ μm. For this reason we can compare the slopes in the experiments performed for similar range of separations.

4.1. *Groningen–Twente group (Au–Au surfaces)*

In these experiments the Casimir/vdW force was measured using the PicoForce AFM[35] in static mode, between an Au coated sphere of diameter 100 μm, and an Au coated silicon plate [Fig. 15(b)]. Both the sphere and plate were coated with 100 nm Au within the same vacuum evaporator. After Au deposition, the rms roughness of sphere and plate were measured by AFM (see Fig. 15) to be ~ 1.8 nm and ~ 1.3 nm respectively. Analysis of the sphere where contact takes place was investigated by inverse AFM imaging [Fig. 15(a)].[35] The contact separation due to roughness d_0 was derived from the top-to-bottom roughness of sphere and plate (from multiple scans at different places of both surfaces) added and divided by two yielding $d_0 = 7.5 \pm 1$ nm.[35]

After calibration, the Casimir force is measured and averaged using 40 force curves. Calibration and measurements were repeated at 20 different locations on the plane having in total an average of 800 curves per sample (averaged for two spheres) to obtain the force in Fig. 16. At separations in the range > 20 nm–100 nm, the force follows the power law with exponent $m = 2.5$. At separations below 20

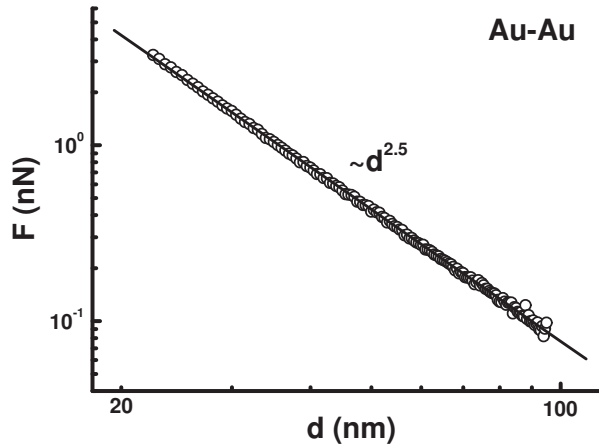

Fig. 16. Force versus separation d from average of 800 independent measurements per sample (also averaged for two different spheres) with the power laws indicated for vdW and Casimir regimes.[35]

nm, retardation effects begin to diminish entering the force regime known as the vdW force regime.

4.2. *Purdue group (Au–Au surfaces)*

In this experiment[38] the Casimir pressure between two Au-coated parallel plate surfaces was determined dynamically by means of a micromechanical torsional oscillator consisting of a plate suspended at two opposite points by serpentine springs, and a sphere above it attached to an optical fiber (all details of the experimental setup are presented in Ref. 39). The thickness of the Au coating was 210 nm. The micromachined oscillator and the sphere with a fiber were mounted inside a can with magnetic damping vibration isolation, where a pressure below 10^{-4} Torr was maintained.[38,39] The sphere that was used had the size $R = 151.3$ μm. The rms roughness of both Au coated sphere and plate were less than 3 nm.

What is actually measured in this experiment was the Casimir pressure which is defined via the force derivative $\partial F(d)/\partial d$

$$P(d) = \frac{1}{2\pi R}\frac{\partial F}{\partial d}\,. \tag{4.2}$$

In the separation range $\sim$160–500 nm the Casimir pressure follows the power law behaviour with the exponent $1 + m = 3.71$ or $m = 2.71$ [Fig. 17(a)], while above 500 nm the slope was slightly increased to $1 + m = 3.84$ or $m = 2.84$ [Fig. 17(b)]. A fit over the whole range $\sim$160–750 nm yielded $1 + m = 3.76$ or $m = 2.76$ [Fig. 17(c)].

4.3. *Grenoble group (Au–Au surfaces)*

In this experiment[40] a 20 μm radius sphere was glued to the end of an AFM cantilever forming the force probe. The latter, which can be considered as a harmonic

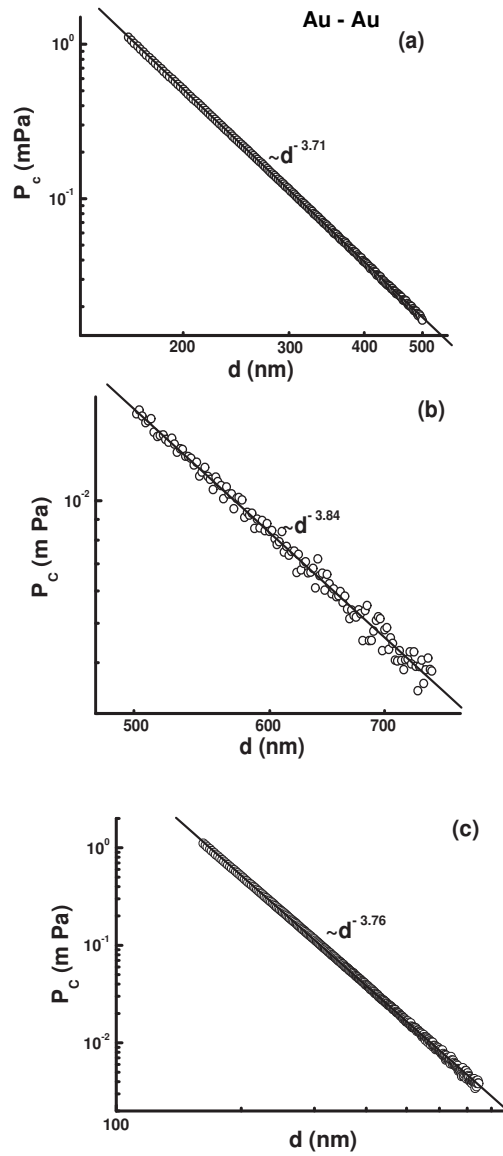

Fig. 17. Casimir pressure as a function of separation d. (a) separation range 160–500 nm, (b) above 500 nm. Data courtesy of R. Decca. (c) The whole range of separation gives an average exponent $m = 2.75$.

oscillator, is mechanically excited at its free resonance frequency and the force gradient (Fig. 18) is measured as in Ref. 38. The Casimir force arises between the bottom part of the microsphere coated with 300 nm Au and a flat gold surface. The roughness of the two interacting surfaces were respectively lower than 3 nm rms. In the separation range $\sim$98–300 nm the Casimir pressure follows the power

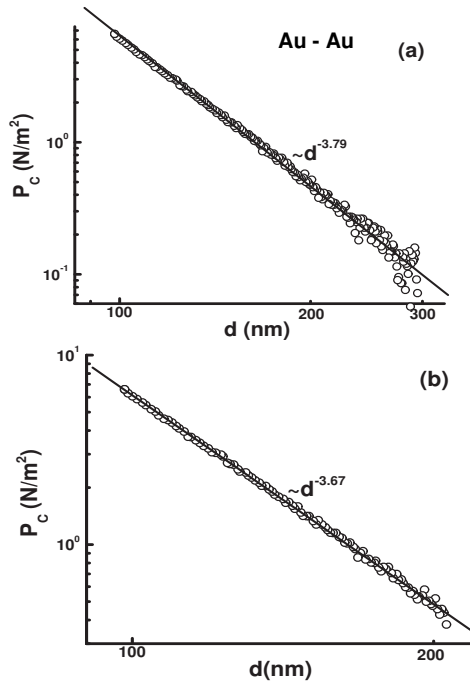

Fig. 18. (a) Casimir pressure versus separation in the range 98–300 nm, (b) similar plot but limited in the range 98–200 nm. Data courtesy of J. Chevrier, J. Laurent, and H. Sellier.

law with exponent, $1 + m = 3.79$ or $m = 2.79$ [Fig. 18(a)], while below 200 nm the scaling exponent appeared to be slightly decreased to the value $1 + m = 3.67$ or $m = 2.67$.

4.4. *Yale group (Ge–Ge surfaces)*

In this experiment[41] using the well-known torsion balance setup, the Casimir force was measured between crystalline Ge plates in a sphere-plane geometry. On one side of a torsion pendulum, a flat Ge plate is mounted, and approached by a Ge plate with a spherical surface having radius of curvature $R = 15$ cm. The Casimir force after subtraction of the electrostatic force is shown in Fig. 19. The force data shows in the range 550–1500 nm a power law behaviour with exponent $m = 2.84$. The complete force measurement range was in the range 550–72900 nm (Fig. 19). However, since electrostatics remained a significant problem at larger separations (> 2000 nm), it was decided not to further analyse this range.

4.5. *Amsterdam group (Au-ITO surfaces)*

In this experiment[42] an ITO coating (conductive Indium-Tin-oxide) as one of the two interacting surfaces was used.

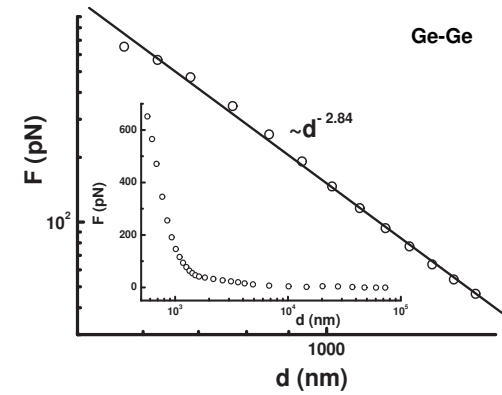

Fig. 19. Force measurements in the range 550–1500 nm and a power-law fit. The inset shows the data over the whole range of separations up to 72900 nm. Data courtesy of S. Lanoreaux and D. Dalvit.

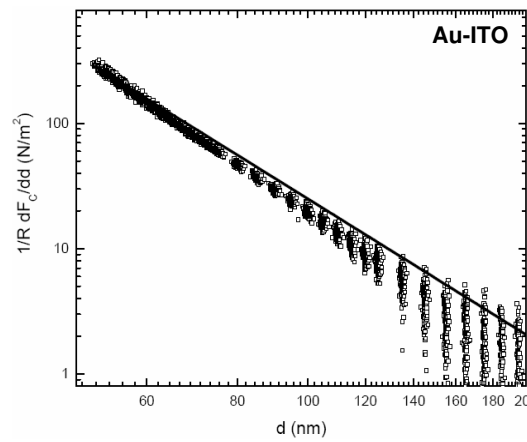

Fig. 20. Casimir pressure measurements for the Au-ITO systems.[42] Figure courtesy of S. De-Maan.

Since ITO was transparent over a wide range of frequencies, the Casimir attraction was found to be a factor of 2 smaller than that of the Au–Au interaction. Also, here the force measurement was performed with a dynamic mode based AFM technique using spheres with radius $R = 100$ μm. Measurement of the scaling exponent of the Casimir pressure at separations $d > 70$ nm (to avoid any roughness influence) yielded $1 + m = 3.75$ or $m = 2.75$ (Fig. 20).[43]

4.6. *Leicester–Groningen–Twente groups (Au-AIST surfaces)*

In this experiment[44] a controllable variation in the Casimir force was demonstrated. Changes in the force of up to 25% at separations of ~ 100 nm between Au and

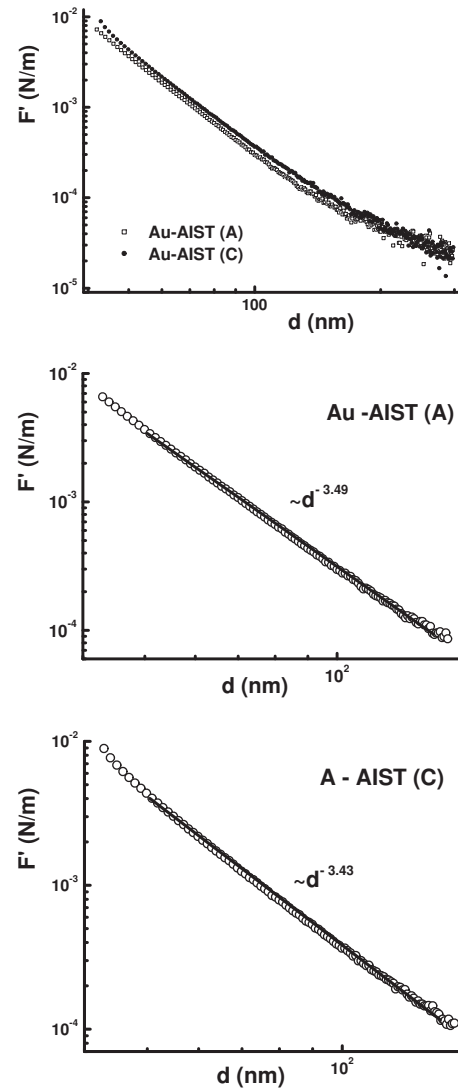

Fig. 21. Gradient force (F') curves versus separation d for the system (top) Au-AIST, (middle) Au-amorphous AIST (A) and (bottom) Au-crystalline AIST (C) in the separation range 55–130 nm. We fitted the data above the separation of 50 nm to avoid any roughness influence and below 130 nm in order to avoid any noisy data at larger separations (>150 nm).

AgInSbTe (AIST) surfaces were achieved by switching between amorphous and crystalline phase samples of AIST. The material is well-known for its structural transformation, which produces a significant change in the optical properties, and is exploited in optical data storage systems. The force gradient was measured using the dynamic mode in an ultra-high-vacuum AFM. The force results are shown in Fig. 21.

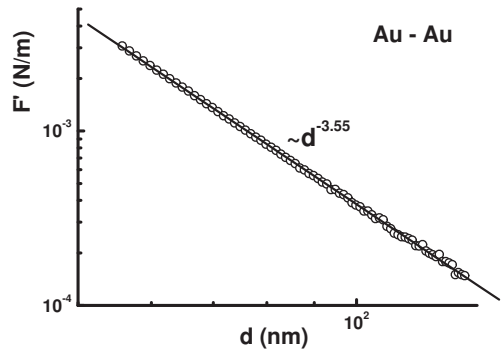

Fig. 22. Gradient force (F') curves versus separation d (top) for the system Au–Au using the same sphere for Au-AIST measurements shown in Fig. 21. The linear fit is in the range 55–130 nm as calculated previously for the AIST films. The force gradient is expressed in Hz since it is proportional to change in frequency in dynamic mode AFM force measurements. Data courtesy of G. Toricelli and C. Binns.

Determination of the scaling exponent of the Casimir force gradient ($F' = \partial F/\partial d$) was performed at separations $d > 50$ nm to avoid any roughness influence, and up to 120 nm to avoid the influence of increased data noise at larger separations as the top schematic in Fig. 21 shows. The fits yielded the exponents $1 + m = 3.39$ or $m = 2.49$ for the Au-AIST (amorphous), and $1 + m = 3.43$ or $m = 2.43$ for the Au-AIST (crystalline) system.[44]

Finally, we show in Fig. 22 for comparison the Au–Au data obtained using the same Au coated sphere. The corresponding linear fit yields for the Casimir force gradient at separations 55–130 nm the exponents $1 + m = 3.55$ or $m = 2.55$.

4.7. *Leicester group (Au–Au and Au-HOPG surfaces)*

In this experiment[46] a significant difference between Au–Au and Au-HOPG (highly oriented pyrolytic graphite) was demonstrated. The force gradient was measured using dynamic mode in an ultra-high-vacuum AFM as in Sec. 4.6. The force results are shown in Fig. 23. The force data is shown as a frequency shift Δf which is proportional to the force gradient; $\Delta f \sim \partial F/\partial d$. Determination of the scaling exponent of the Casimir force gradient ($F' = \partial F/\partial d$) was performed at separations $d > 65$ nm (to avoid any roughness influence; and up to 350 nm to keep minimum influence of increased data noise). For the Au–Au system, the exponent $1 + m = 3.61$ or $m = 2.61$ was obtained using one of the available set of data, while for Au-HOPG, it was found that $1 + m = 3.47$ or $m = 2.47$.

4.8. *Dartmouth-Padova group (Au–Au surfaces)*

In this experiment[47,48] forces are acting between two macroscopic conducting surfaces in a sphere-plane configuration (Fig. 24). Below a cantilever, a spherical mirror of radius $R = 3.9$ mm and diameter $a = 8$ mm was mounted on an aluminium frame

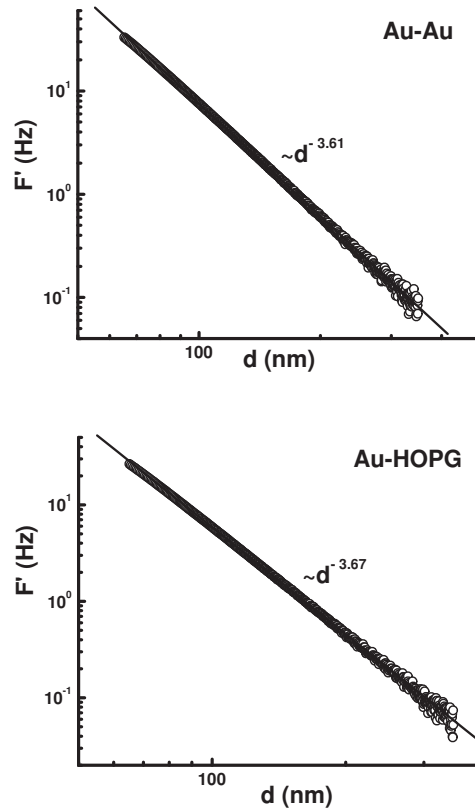

Fig. 23. Gradient force curves versus separation d for the systems (top) Au–Au and (bottom) Au-HOPG. The force gradient is expressed in Hz since it is proportional to change in frequency in dynamic mode AFM force measurements. Data courtesy of G. Toricelli and C. Binns.

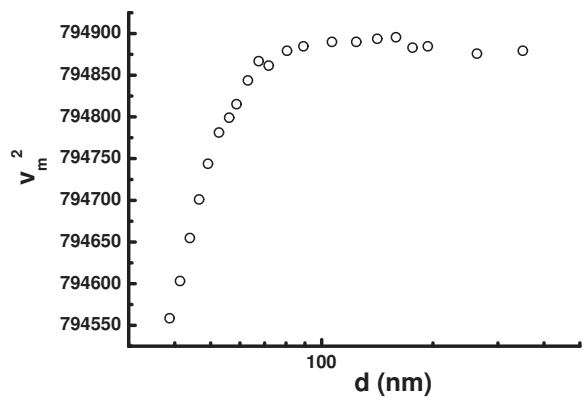

Fig. 24. Squared frequency (Hz^2) of the cantilever versus separation d. After subtracting the electrostatic residuals the Casimir force was evidently corresponding to exponents less than 4. Data courtesy of W. J. Kim and R. Onofrio.

connected to two motorized actuators. The spherical lens was Au coated with thickness of 250 nm. Finally the measurements were obtained by performing electrostatic calibrations followed by a residuals analysis after subtracting the electrostatic-dependent component. In spite of electrostatic anomalies, evidence was found for short-distance attractive forces of magnitude comparable to the expected Casimir–Lifshitz force.[47,48] The relevance of these findings using a macroscopic size system was discussed in the more general context of Casimir–Lifshitz force measurements, with particular regard to the critical issues of the electrical and geometrical characterization of the involved surfaces. Disentangling forces of different origins as it is shown in this work became exceedingly complex with the unexpected power law found in the electrostatic analysis for this system. Preliminary residual fitting indicated exponents for the frequency shift, which is proportional to the Casimir force gradient, $1 + m = 3.64$ or equivalently $m = 2.64$.[49,50]

4.9. *Summary of all force results*

All the results from the various groups are summarized in Table 2. From this table, it is evident that the presented data span a rather wide range of materials from metals to semiconductors. From direct comparison it becomes clear that the exponent m of the Casimir force, $F \propto d^{-m}$, was in all cases lower than 3. The latter represents the case of perfectly reflecting mirrors for the sphere-plate geometry. Over the whole separation range 20–1500 nm, for measurements performed at room temperature ($T \approx 300$ K), in air or vacuum as the intervening medium, the exponent m appears to span the range $m \approx 2.65 \pm 0.2$. This value deviates consid-

Table 2. The scaling exponent m of the Casimir force versus separation distance, $F \sim d^{-m}$ for the sphere-plate geometry showing also the corresponding separation distance. Although error bars are not stated, in all cases the statistical error for the exponent m was ≤ 0.05.

Interacting materials/surfaces	Separation range	Exponent m
Au–Au[35]	25–100 nm	$m = 2.5$
Au–Au[38]	160–500 nm	$m = 2.71$
	500–750 nm	$m = 2.84$
	160–750 nm	$m = 2.76$
Au–Au[40]	98–300 nm	$m = 2.79$
	98–200 nm	$m = 2.67$
Ge–Ge[41]	550–1500 nm	$m = 2.84$
Au–ITO[42]	70–200 nm	$m = 2.75$
Au–AIST (A)[43]	55–130 nm	$m = 2.49$
Au–AIST (C)[43]	55–130 nm	$m = 2.43$
Au–Au[43]	55–130 nm	$m = 2.55$
Au–Au[45,46]	65–350 nm	$m = 2.61$
Au–HOPG[45,46]	65–350 nm	$m = 2.67$
Au–Au[47–50]	30–1000 nm	$m = 2.64$

erably from $m = 3$ for ideal metals. It means that the particular optical properties of real materials play significant role in determining dispersive forces. Moreover, comparing the results obtained from different groups, it becomes clear that there is good agreement indicating that a strong consensus in the Casimir field has been reached. This is clearly shown, for example, from the Au–Au force data, which is the most common measurement system of interacting material surfaces.

5. Conclusion

Casimir and van der Waals dispersive forces between macroscopic surfaces are strongly influenced at small surface separations (smaller than the plasma wavelength λ_p) by surface roughness and the frequency dependent dielectric functions of the interacting materials. Lifshitz theory allows calculations of the Casimir/vdW force only between two flat plates given that the frequency dependent dielectric function is known. Indeed, we cannot compare different measurements of the Casimir force with accuracy below the force uncertainty arising as a result from the known variation in dielectric data of a given material. Therefore, when we are dealing with dispersive forces between real materials precise characterization of the particular samples is critical. As a result the effects of roughness and optical properties on the Casimir/vdW force were discussed in this review paper. Moreover, in the regime of separations where beyond surface roughness plays no role, comparing the results obtained from different groups, it becomes clear that there is good agreement indicating that a strong consensus in the Casimir field has been reached. Notably, over the whole separation range 20–1500 nm, for measurements performed at room temperature ($T \approx 300$ K), in air or vacuum as the intervening medium, the average exponent m of the Casimir force appeared to span the range $m = 2.65 \pm 0.2$. The latter clearly shows that $m < 3$, which is in agreement with expectations for real materials having finite conductivity.

Acknowledgments

We would like to thank R. Decca, D. Dalvit, S. Lanoreaux, J. Chevrier, J. Laurent, H. Sellier, S. DeMaan, G. Toricelli, C. Binns, R. Onofrio and W. J. Kim for providing their data and figures for this review article. G. Palasantzas and P. J. van Zwol would like to acknowledge support from Project No. MC3.05242 of the research program of the Materials Innovation Institute M2i. The authors benefited from exchange of ideas with the ESF Research Network CASIMIR.

References

1. H. B. G. Casimir and D. Polder, *Phys. Rev.* **73**, 4 (1948).
2. H. B. G. Casimir *Proc. KNAW* **51**, 793 (1948).
3. E. M. Lifshitz, *Sov. Phys. JETP* **2**, 73 (1956); I. E. Dzyaloshinskii, E. M. Lifshitz and L. P. Pitaevskii, *Adv. Phys.* **10**, 165 (1961).

4. S. K. Lamoreaux, *Phys. Rev. Lett.* **78**, 5 (1997); S. K. Lamoreaux, *Rep. Prog. Phys.* **68**, 201 (2005).
5. B. W. Harris *et al.*, *Phys. Rev. A* **62**, 052109 (2000); M. Bordag *et al.*, *Phys. Rep.* 353 (2001); P. J. van Zwol *et al.*, *Phys. Rev. B* **77**, 075412, (2008); S. DeMaan *et al.*, *Phys. Rev. Lett.* **103**, 040402 (2009); G. Jourdan *et al.*, *EPL* **85**, 31001 (2009).
6. P. A. Maia Neto, A. Lambrecht and S. Reynaud, *Phys. Rev. A* **72**, 012115 (2005).
7. I. Pirozhenko, A. Lambrecht and V. B. Svetovoy, *New J. Phys.* **8**, 238 (2006).
8. V. B. Svetovoy, P. J. van Zwol, G. Palasantzas *et al.*, *Phys. Rev. B* **77**, 035439 (2008).
9. N. Yoshimatsu *et al.*, *e-J. Surf. Sci. Nanotech.* **3**, 524 (2005).
10. P. Romaniello and P. L. de Boeij, *J. Chem. Phys.* **122**, 164303 (2005).
11. T. Y. Tan *et al.*, *Appl. Phys. Lett.* **30**, 175 (1977).
12. R. S. Decca *et al.*, *Phys. Rev. D* **75**, 077101 (2007).
13. E. D. Palik, *Handbook of Optical Constants of Solids* (Academic, New York, 1995).
14. J. H. Weaver *et al.*, *Optical Properties of Metals, Part II, Physics Data No. 18-2* (Fachinformationszentrum Energie, Physik, Mathematik, Karlsruhe, 1981).
15. S. K. Lamoreaux, *Phys. Rev. A* **59**, R3149 (1999).
16. P. J. van Zwol and G. Palasantzas, *Phys. Rev. B* **79**, 195428 (2009).
17. R. M. A. Azzam and N. M. Bashara, *Ellipsometry and Polarized Light* (North Holland, Amsterdam, 1987).
18. H. G. Tompkins and W. A. McGahan, *Spectroscopic Ellipsometry and Reflectometry* (Wiley, New York, 1999).
19. T. Hofmann *et al.*, *Mater. Res. Soc. Symp. Proc.* **1108**, A08-04 (2009).
20. R. Feng and C. E. Brion, *Chem. Phys.* **282**, 419 (2002).
21. H. G. Tompkins and E. A. Irene, *Handbook of Ellipsometry* (William Andrew, New York, 2005).
22. A. Lambrecht and S. Reynaud, *Eur. Phys. J. D* **8**, 309 (2000).
23. P. A. Maia Neto *et al.*, *Phys. Rev. A* **72**, 012115 (2005).
24. P. J. van Zwol, G. Palasantzas and J. Th. M. DeHosson, *Phys. Rev. B* **77**, 075412 (2008).
25. M. Bordag *et al.*, *Phys. Rep.* **353** (2001).
26. G. Palasantzas, *J. Appl. Phys.* **97**, 126104 (2005).
27. P. J. van Zwol *et al.*, *Appl. Phys. Lett.* **91**, 144108 (2007).
28. J. Krim and G. Palasantzas, *Int. J. Mod. Phys. B* **9**, 599 (1995).
29. G. Palasantzas, *Phys. Rev. B* **48**, 14472 (1993); **49**, 5785 (1994).
30. Y. P. Zhao *et. al.*, *Characterization of Amorphous and Crystalline Rough Surfaces — Principles and Applications* (Academic Press, San Diego, 2001).
31. P. J. van Zwol, V. B. Svetovoy and G. Palasantzas, *Phys. Rev. B* **80**, 235401 (2009).
32. F. W. DelRio *et al.*, *Appl. Phys. Lett.* **90**, 163104 (2007).
33. P. J. van Zwol *et al.*, *Appl. Phys. Lett.* **91**, 101905 (2007).
34. P. J. van Zwol *et al.*, *Phys. Rev. E* **78**, 031606 (2008).
35. P. J. van Zwol, G. Palasantzas, M. van de Schootbrugge and J. Th. M. DeHosson, *Appl. Phys. Lett.* **92**, 054101 (2008); G. Palasantzas, P. J. van Zwol and J. Th. M. DeHosson, *Appl. Phys. Lett.* **93**, 121912 (2008).
36. G. Palasantzas, V. B. Svetovoy and P. J. van Zwol, *Phys. Rev. B* **79**, 235434 (2009).
37. S. deMaan *et al.*, *Phys. Rev. Lett.* **103**, 040402 (2009).
38. R. S. Decca, D. López, E. Fischbach, G. L. Klimchitskaya, D. E. Krause and V. M. Mostepanenko, *Phys. Rev. D* **75**, 077101 (2007); R. S. Decca, D. López, E. Fischbach, G. L. Klimchitskaya, D. E. Krause and V. M. Mostepanenko, *Eur. Phys. J. C* **51**, 963 (2007).
39. R. S. Decca *et al.*, *Ann. Phys.* **318**, 37 (2005).

40. G. Jourdan, A. Lambrecht, F. Comin and J. Chevrier, *EPL* **85**, 31001 (2009).
41. W. J. Kim, A. O. Sushkov, D. A. R. Dalvit and S. K. Lamoreaux, *Phys. Rev. Lett.* **103**, 060401 (2009).
42. S. de Maan, K. Heeck, R. J. Wijngaarden and D. Iannuzzi, *Phys. Rev. Lett.* **103**, 040402 (2009).
43. S. de Maan, unpublished, private communications.
44. G. Torricelli, P. J. van Zwol, A. Shpak, C. Binns, G. Palasantzas, B. Kooi, V. B. Svetovoy and M. Wuttig, *Phys. Rev. A* **82**, 010101 (RC) (2010).
45. G. Torricelli, S. Thornton, C. Binns, I. Pirozhenko and A. Lambrecht, *J. Vac. Sci. Technol. B* **28**, C4A30 (2010).
46. G. Torricelli *et al.*, *J. Vac. Soc. B* (to be published).
47. W. J. Kim, M. Brown-Hayes, D. A. R. Dalvit, J. H. Brownell and R. Onofrio, *Phys. Rev. A* **78**, 020101 (2008).
48. W. J. Kim, M. Brown-Hayes, D. A. R. Dalvit, J. H. Brownell and R. Onofrio, *J. Phys.: Conf. Series* **161**, 012004 (2009).
49. W. J. Kim, Ph.D. thesis, Dartmouth College, 2007 (unpublished).
50. W. J. Kim et al. (unpublished).